Theoretical and Experimental Aerodynamics of the Sailwing

ROBERT A. ORMISTON*
Department of the Navy, Ames Research Center, Moffett Field, Calif.

The sailwing is a unique type of semiflexible foldable wing. A brief description of its construction, basic properties, and some past research, is used to introduce an analytical and experimental study of its aerodynamic characteristics. Emphasis is placed on an approximate structural analysis which treats the nonlinear behavior of the sail deflection. Two-dimensional flexible airfoil theory and Prandtl lifting-line theory are used to establish the aerodynamic loading. The results allow prediction of the induced tensions, the nonlinear life curve, induced drag, and aeroelastic divergence of the sail chordwise deflection mode. Selected experimental results are presented for comparison with the theory, along with a brief discussion of the implications of the study regarding flight vehicle applications of the sailwing.

Nomenclature

AR = aspect ratio
b,c = span, chord, ft
c_l = two-dimensional lift coefficient
c_γ = sail-deflection parameter, Eq. (32)
C_L = lift coefficient
C_{L_α} = angle-of-attack lift effectiveness, per rad
$C_{L_{\bar{\alpha}_s}}$ = sail angle lift effectiveness, per rad
C_{T_o} = tension coefficient, T_o/qS_w
$C_{T_{od}}$ = divergence tension coefficient
G = membrane deflection parameter, Eq. (32)
K_ϵ = camber lift effectiveness, $7.28/2\pi$
K = elastic constant, lb/ft, lb/ft²
l = length, ft
L = lift, lb
N_w,N_s = Stiffness numbers, Eqs. (28) and (29)
n = harmonic number
P = pressure, lb/ft²
q = dynamic pressure, lb/ft²
R_o,R_k = Stiffness numbers, Eq. (28)
S_w = wing area, ft²
$t,\Delta t$ = membrane tension, lb/ft
$T,T_o,\Delta T$ = trailing-edge tension, lb
u,v,z = membrane displacements in x, y, and vertical directions, ft.
$x_t,x_{to},\Delta x_t$ = trailing-edge chordwise deflections, (Fig. 4a)
z_o = nondimensional sail deflection at mid-semispan, ft
z_t = trailing-edge vertical deflection, ft
α_s = sail effective angle of attack, rad
α_T = angle of attack due to trailing edge, rad
α_ϵ = angle of attack due to camber, rad
β = trailing-edge design shape parameter, rad
γ = membrane parameter, Eq. (32)
δ = induced drag factor
δ_o = trailing-edge parameter, $\beta b/8$ (Fig. 4a)
ϵ = membrane strain
$\bar{\epsilon}$ = slackness ratio
ξ = nondimensional membrane deflection, z/c
ζ,η = nondimensional chordwise and spanwise coordinates, x/c, $y/b/2$
σ = membrane induced tension, lb/ft
ψ = aerodynamic parameter, Eq. (49)

Superscripts

$(^-)$ = nondimensional variable
$(')$ = differentiation

Subscripts

x = chordwise
y = spanwise
o = initial
11 = first harmonic of double Fourier series
s = sail
w = trailing wire

Received December 29, 1970; revision received May 28, 1970.

* Research Scientist, U. S. Army Air Mobility Research & Development Laboratory Ames Directorate. Member AIAA.

1. Introduction

THE sailwing is a unique type of semiflexible, foldable wing which has been under development at Princeton University since 1948.[1] The purpose of this paper is to describe its aerodynamic features and present the results of a recent research investigation of the sailwing.[2] To acquaint the reader with the fundamentals of the sailwing configuration, a schematic picture is given in Fig. 1. A leading-edge spar with attached ribs forms an ideally rigid framework which supports a trailing-edge tension cable. A membrane (usually dacron) is wrapped around the leading edge and attached to the trailing-edge, forming the upper and lower sail surfaces. The shape of the pre-tensioned trailing-edge member is designed to impart a chordwise tension in the membrane to minimize deflections due to aerodynamic loads. In addition to the high aspect ratio planform, this results in a wing with excellent maximum lift-drag ratios. The practical potential of the sailwing has spurred experimental and analytical research in many areas,[1-8] including aerodynamics, longitudinal stability and lateral control. Possible applications such as auxiliary wings for air cushion vehicles, towed cargo gliders, foldable light aircraft, rocket booster recovery aids, lifting body re-entry vehicles, and compound helicopters have been studied.

Aerodynamic Features

In contrast with most flexible wings, the aerodynamic features of the sailwing are substantially similar to conventional rigid wings. A typical lift coefficient vs angle-of-attack curve for a sailwing at constant dynamic pressure is illustrated in Fig. 2. A comparable rigid wing curve is shown by the dotted line. In comparison, the sailwing exhibits a higher slope which is attributable to the rate of change of camber (membrane deflection) with angle of attack. The pronounced nonlinearity results from induced tension in the

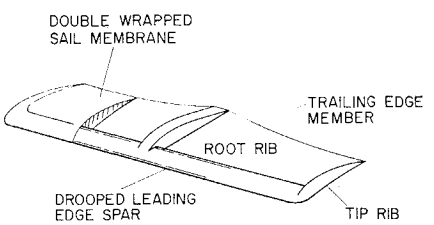

Fig. 1 Sailwing construction features.

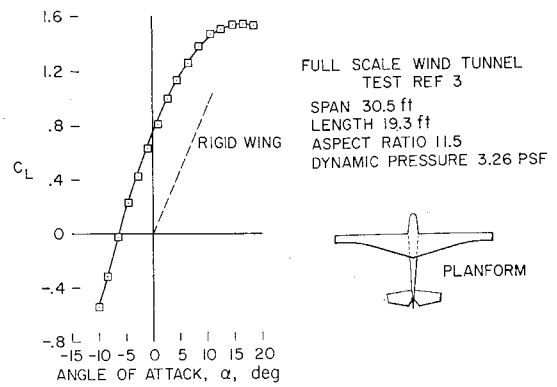

Fig. 2 Typical sailwing aerodynamic characteristics.

membrane which increases its resistance to deflection as angle of attack increases.

With this simplified explanation, it is apparent that the details of sailwing aerodynamics are intimately related to a variety of parameters, such as angle of attack, dynamic pressure, sail and trailing-edge pretension, and the elastic properties of these components.

It might be expected that the spanwise variation of twist, resulting from vertical deflection of the trailing-edge (note deflections of the wing frame are not considered) and camber would significantly alter the spanwise lift distribution and hence, increase the induced drag of the sailwing. Although this is a legitimate fundamental question, experimental measurements show no significant reduction in maximum lift-drag ratio. Figure 3 is intended to illustrate this point and especially to contrast sailwing performance with other types of flexible wings. This plot compares experimental data with the performance of a nominal rigid wing. The sailwing is seen to be substantially comparable to the rigid wing, whereas other types[9–15] are compromised by the effects of deformation. It can be seen that as the degree of flexibility is increased, the effects of deformation are more severe, and in addition, the maximum practical aspect ratios are reduced.

An area of special concern with the sailwing is aeroelastic instability of the sail surface. In contrast with most flexible wings which rely on a positive lift load to maintain a stable deflection of the lifting surface, the sailwing also gains stability from the internal membrane tension produced by the trailing-edge cable. This allows the sailwing to operate through conditions of positive and negative lift unlike non-pre-tensioned flexible wings. In certain cases however, at high dynamic pressure or low pre-tension, the sailwing is subject to membrane instabilities near the point of zero lift. Because of the strong influence of the nonlinear effects under these conditions, the instabilities are manifest in the form of hysteresis loops in the lift curve in the neighborhood of zero lift.

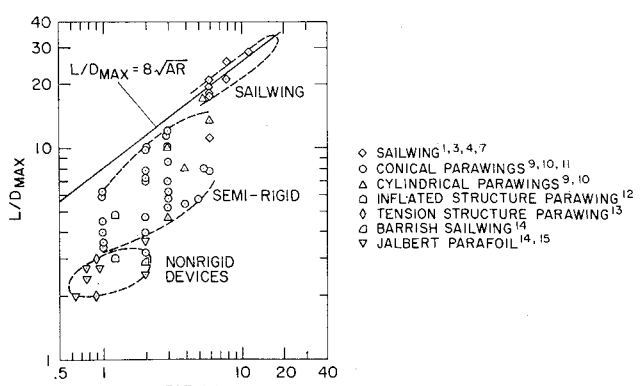

Fig. 3 Comparison of maximum lift-drag ratios of various types of flexible wings with a nominal rigid wing.

Scope of Study

The increasing interest in applications of the sailwing previously mentioned underscores the need for rational analytical methods to understand and predict aerodynamic and aeroelastic properties. The theory begins in section 2 with a structural analysis of the sailwing, with particular emphasis placed on the nonlinear aspects. In section 3, the three-dimensional aerodynamic characteristics determined from Prandtl lifting-line theory are discussed. The mutual coupling between the aerodynamic loads and the sail structural deflections is developed in section 4. In addition, the conditions for aeroelastic divergence, and the relations for the nonlinear lift curve are presented. Some experimental measurements are presented in section 5. Since certain analytical results could be seen to have a direct bearing on applications of the sailwing to flight vehicles, a brief discussion of their ramifications is given in section 6, and conclusions are given in section 7.

2. Structural Analysis

Sail Membrane

This portion of the analysis considers the elastic deflections and induced tensions of the sail and trailing-edge members which support the sailwing airload. Figure 4a illustrates the coordinate systems and geometry of an idealized rectangular sailwing with a single sail surface. The sail deflection is given by $z(x,y)$, whereas the trailing-edge vertical and chordwise deflections are given by $z_t(y)$ and $x_t(y)$, respectively. For the idealized sailwing considered here, spar and tip rib deflections are not considered. Note that the trailing-edge design shape is produced by a balance of the trailing-edge pre-tension and chordwise membrane pre-tension at zero lift. It is characterized by the geometric parameter β, which will be defined below.

The membrane deflection equation is

$$t_x(\partial^2 z/\partial x^2) + t_y(\partial^2 z/\partial y^2) = -P(x,y) \qquad (1)$$

where the airload distribution is $P(x,y)$ and t_x and t_y are the

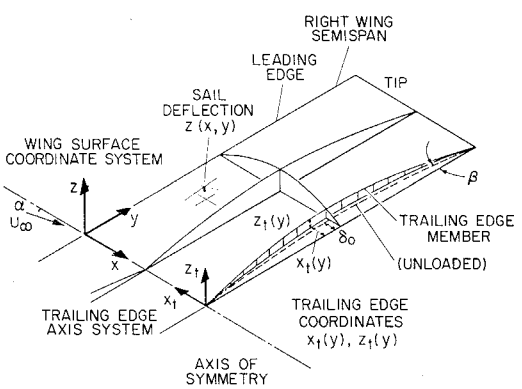

a) Coordinate systems for sail and trailing-edge deflections

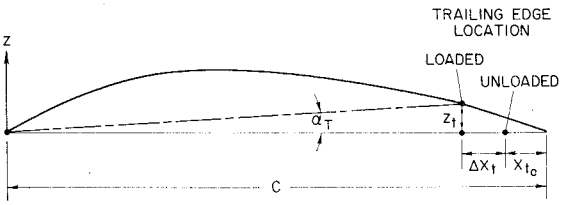

b) Local camber and twist induced by sail and trailing-edge deflection

Fig. 4 Sailwing geometry.

chordwise and spanwise tensions in the membrane. A term due to shear stress, $2\tau_{xy}(\partial^2 z/\partial x \partial y)$, is here neglected for simplicity, which is permissible because t_x and t_y contain significant pre-tension contributions. The associated chordwise and spanwise membrane strains, including the nonlinear terms are next given:

$$\epsilon_x = \partial u/\partial x + \tfrac{1}{2}(\partial z/\partial x)^2 \quad (2)$$

$$\epsilon_y = \partial v/\partial y + \tfrac{1}{2}(\partial z/\partial y)^2 \quad (3)$$

The membrane tensions t_x and t_y consist of pre-tensions and induced tensions resulting from deflection of the sail under load:

$$t_x = t_{x_o} + \sigma_x \quad (4)$$

$$t_y = t_{y_o} + \sigma_y \quad (5)$$

For the present study we will assume that woven sail materials obey Hooke's law and that Poisson's ratio μ can be taken to be zero. The induced tensions σ_x and σ_y are then directly proportional to the sail elongations in the x and y directions, respectively, where K_x and K_y are the associated elastic constants:

$$\sigma_x = K_x \Delta l_x \quad (6)$$

$$\sigma_y = K_y \Delta l_y \quad (7)$$

The elongations may be derived by integrating the equations for strain and accounting for the displacement of the membrane boundary Δx_t. We then have

$$\sigma_x = K_x\left[\frac{1}{2}\int_0^c \left(\frac{\partial z}{\partial x}\right)^2 dx - \Delta x_t\right] \quad (8)$$

$$\sigma_y = \frac{K_y}{2}\int_0^{b/2}\left(\frac{\partial z}{\partial y}\right)^2 dy \quad (9)$$

The induced tensions are functions of the membrane deflection and thus, clearly illustrate the nonlinear mathematical nature of the sailwing structural system. This is because the partial derivatives of the deflections in Eq. (1) are multiplied by the membrane tensions (t_x and t_y), which themselves contain the deflections.

Trailing-Edge Transverse Deflections

First consider the trailing-edge deflection x_{t_o} (design shape) due to pre-tension at zero lift:

$$x_{t_o} = (2\beta/b)y(b/2 - y),\ \beta = bt_{x_o}/4T_o \quad (10)$$

For lifting conditions, the trailing edge chordwise position is given by

$$x_t = x_{t_o} + \Delta x_t \quad (11)$$

The trailing-edge loading is the reaction to the horizontal component of the sail membrane chordwise tension. For small deflections, the deflection equation for a loaded cable is

$$x_t'' = -(t_{x_o} + \sigma_x)/T,\ T = T_o + \Delta T \quad (12)$$

where T_o is the pre-tension and ΔT the induced tension of the trailing-edge cable. Combining Eqs. (10–12), we have the differential equation for the increment of trailing-edge deflection due to the airload:

$$\Delta x_t'' = [t_{x_o}\Delta T/T_o - \sigma_x(y)]/T \quad (13)$$

Rather than develop the analogous equation for the vertical deflection of the trailing edge, we will resort to a useful approximation for simplicity:

$$z_t(y) = z[(c - x_t), y] \quad (14)$$

This equation states that the vertical deflection of the trailing edge is equal to the sail deflection at the locus of points described by the chordwise position of the trailing edge x_t.

Trailing-Edge Elongation

A significant effect of the trailing-edge transverse deflection is the associated elongation Δl. The resulting tension is referred to as the trailing-edge induced tension:

$$\Delta l = l - l_o \quad (15)$$

K_w is the elastic constant and l_o is the length at zero lift, resulting from the trailing-edge design shape, Eq. (10),

$$l_o = \int_0^{b/2}[1 + (x_{t_o}')^2]^{1/2} dy \quad (16)$$

The length under load is

$$l = \int_0^{b/2}[1 + (x_t')^2 + (z_t')^2]^{1/2} dy \quad (17)$$

Combining these equations,

$$\Delta T = \frac{K_w}{2}\int_0^{b/2}[(\Delta x_t')^2 + 2\Delta x_t' x_{t_o}' + (z_t')^2] dy \quad (18)$$

Solution for the Induced Tensions

The aforementioned equations are first nondimensionalized in the following way. Sail- and trailing-edge deflections are divided by the chord $z/c = \zeta$, $x_t/c = \bar{x}_t$, $z_t/c = \bar{z}_t$, the chordwise coordinate is $\xi = x/c$, the spanwise coordinate is $\eta = y/b/2$. Tensions are divided by their respective pre-tensions; $t_x/t_{x_o} = \bar{t}_x$, $t_y/t_{y_o} = \bar{t}_y$, $T/T_o = \bar{T}$, $\sigma_x/t_{x_o} = \bar{\sigma}_x$, $\sigma_y/t_{y_o} = \bar{\sigma}_y$, $\Delta T/T_o = \Delta\bar{T}$, and lift by T_o, $\bar{L} = L/T_o$. $\bar{P}(\xi, \eta)$ refers to the normalized pressure distribution $\bar{P} = P/L$. The complete set of equations then becomes

$$\bar{\sigma}_x(\eta) = AR^{1/2}\left[\tfrac{1}{2}\int_0^1 \left(\frac{\partial\zeta}{\partial\xi}\right)^2 d\xi - \Delta\bar{x}_t\right]\Big/ 4\beta N_s \quad (19)$$

$$\bar{\sigma}_y(\xi) = \left[\int_0^1 \left(\frac{\partial\zeta}{\partial\eta}\right)^2 d\eta\right]\Big/ 2\beta AR^{3/2} R_o N_s \quad (20)$$

$$\bar{t}_x(\partial^2\zeta/\partial\xi^2) + (4R_o/AR^2)\bar{t}_y\partial^2\zeta/\partial\eta^2 = -(\bar{P}(\xi,\eta)/4\beta)\bar{L} \quad (21)$$

$$\bar{z}_t = \zeta(1 - \bar{x}_t, \eta) \quad (22)$$

$$\Delta x_t'' = AR\beta[\Delta\bar{T} - \bar{\sigma}_x(\eta)]/\bar{T} \quad (23)$$

$$\Delta\bar{T} = \left[\int_0^1 [(\Delta\bar{x}_t')^2 + 2\Delta\bar{x}_t'\bar{x}_{t_o}' + (\bar{z}_t')^2] d\eta\right]\Big/ N_w AR^{3/2} \quad (24)$$

The associated auxiliary equations are included next. It will be noted that in Eqs. (25) and (26) the induced tensions have been replaced, for simplicity, by spanwise and chordwise average values:

$$\bar{t}_x = 1 + \Delta\bar{t}_x,\ \Delta\bar{t}_x = \int_0^1 \bar{\sigma}_x(\eta) d\eta \quad (25)$$

$$\bar{t}_y = 1 + \Delta\bar{t}_y,\ \Delta\bar{t}_y = \int_0^1 \bar{\sigma}_y(\xi) d\xi \quad (26)$$

$$\bar{T} = 1 + \Delta\bar{T} \quad (27)$$

These equations represent a coupled nonlinear system which approximates the sailwing structure. Neglecting for the moment the unknown airload distribution $\bar{P}(\xi,\eta)$ and magnitude $\bar{L}$, the six primary unknowns are the induced tensions $\Delta\bar{t}_x$, $\Delta\bar{t}_y$, $\Delta\bar{T}$ and the deflections $\zeta(\xi,\eta)$, $\bar{z}_t$, $\Delta\bar{x}_t$ appearing in the six Eqs. (19–24).

Certain terms appearing in these equations, called Stiffness numbers, are nondimensional parameters incorporating the pre-tension and elastic constants of the sailwing:

$$R_o = t_{y_o}/t_{x_o},\ R_k = K_w/K_s S_w^{1/2},\ N_w = T_o/K_w S_w^{1/2} \quad (28)$$

$$N_s = R_k N_w,\ K_s = AR^{1/2}K_y/2 = K_x/AR^{1/2} \quad (29)$$

It is the nature of the differential Eq. (21) for the membrane that the deflection shape $\zeta(\xi,\eta)$ is relatively insensitive

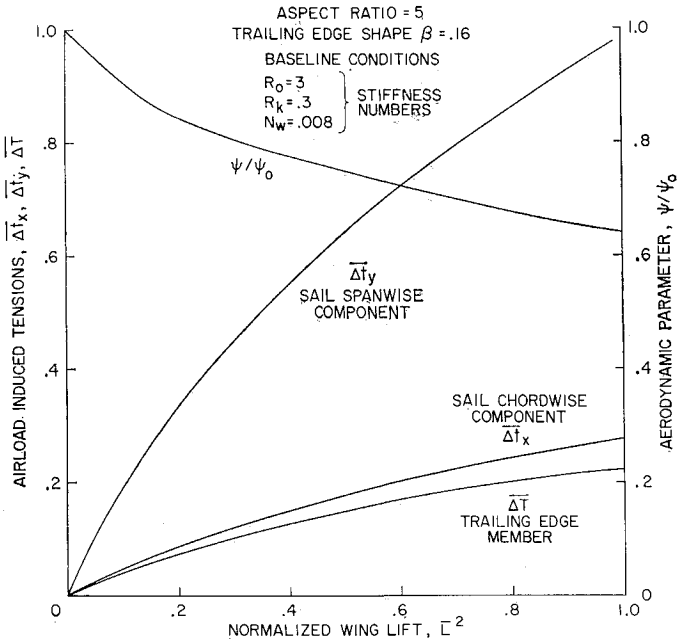

Fig. 5 Spanwise and trailing-edge induced tensions and the aerodynamic parameter ψ/ψ_o.

to the distribution of loading $P(\xi,\eta)$. Considerable simplification can be achieved by approximating the loading by the first term of the Fourier series of a uniform loading and effectively uncoupling the structural problem from the three-dimensional aerodynamic loading equations. Examination of Eqs. (19–27) shows that with the membrane loading and hence, its deflection known, the induced tension and trailing-edge deflection can then be evaluated. Use of a single harmonic term for the loading, and hence, the deflection, insures that the nonlinear portions of the induced equations will be tractable. Proceeding then,

$$\bar{P}(\xi,\eta) = \bar{P}_{11} \sin\pi\eta \sin\pi\xi \tag{30}$$

and using Eq. (21), the membrane deflection is

$$\zeta_{11}(\xi,\eta) = z_o \sin\pi\eta \sin\pi\xi \tag{31}$$

$$z_o = G\bar{L}/4\beta\pi^2\bar{t}_x(1+\gamma^2),\ G = c_\gamma \bar{P}_{11} \tag{32}$$

$$\gamma^2 = (4R_o/AR^2)\bar{t}_x/\bar{t}_y \tag{33}$$

$\bar{P}_{11}$ is given by the formulas for the coefficients of the terms in a Fourier series, and c_γ is a weighting factor that corrects the error in magnitude of the membrane deflection, resulting from using only the first harmonic representation of a uniform loading. In Eq. (32), the lift $\bar{L}$ is not as yet specified, but remains arbitrary. Equation (31) may now be used to evaluate the induced tensions $\Delta\bar{t}_x$, $\Delta\bar{t}_y$, and $\Delta\bar{T}$. The steps of this procedure are given in Ref. 2 and will not be detailed here. The result is

$$\Delta\bar{t}_x = (2\pi^4 N_s^{1/2}\bar{T}^{3/2}/\beta\Lambda R^{7/4})z_o^2 + \Delta\bar{T} \tag{34}$$

$$\Delta\bar{t}_y = \pi^2 z_o^2/8\beta\Lambda R^{3/2}R_o N_s \tag{35}$$

$$\Delta\bar{T} = \frac{2\pi^2\bar{\delta}_o z_o^2}{N_w AR^{3/2}[1+(4\beta^2 R_k/AR)]}\left(1+\frac{\pi^2\bar{\delta}_o}{4}\right) \tag{36}$$

These three simultaneous nonlinear algebraic equations for the membrane chordwise and spanwise induced tension and the trailing-edge induced tension are easily solved by iteration. Typical results are given in Fig. 5. The low values for trailing-edge and chordwise membrane induced tensions in contrast to the spanwise direction, reflect the load relief provided by chordwise movement of the trailing-edge cable. The Stiffness numbers play a prominent role in determining the induced tensions and directly reflect the influence of changes in elastic constants and pre-tensions.

The significance of the sailwing structural properties has been discussed earlier in relation to the nonlinear aerodynamic behavior. The following analyses will incorporate these structural equations in the derivation of the aerodynamic theory. The induced tensions are also important for considerations of sailwing structural design, which will be discussed in section 6.

3. Aerodynamic Analysis

Spanwise Camber and Twist

The previous analysis now permits calculation of the effective camber and aerodynamic twist as a result of the sail and trailing-edge deflection. The forward motion of the trailing edge (Fig. 4b) and the elongation of the sail membrane effectively slacken the sail. This slack manifests itself as curvature of the surface, forming a cambered airfoil section.

The two-dimensional thin airfoil theory applicable to this problem has been developed independently by Thwaites[16] and Nielsen.[17] Nielsen gives a relation for the lift coefficient associated with camber or slackness:

$$c_l = 7.28\bar{\epsilon}^{1/2} - 1.69\alpha\bar{\epsilon}^{1/4} \tag{37}$$

where α is angle of attack and $\bar{\epsilon}$ the slackness ratio,

$$\bar{\epsilon} = (l-c)/c \tag{38}$$

The length of the membrane is l, and the distance between the leading-and trailing-edge attachment points is the chord c. Slackness thus refers to the excess membrane material that is available for curvature or camber. For the present purpose, Eq. (37) can be simplified with little loss in accuracy;

$$c_l = 7.28\bar{\epsilon}^{1/2} \tag{39}$$

Now, including the lift due to angle of attack,

$$c_l = 2\pi(K_\epsilon\bar{\epsilon}^{1/2} + \alpha),\ K_\epsilon = 7.28/2\pi \tag{40}$$

For the present case, the slackness ratio is

$$\bar{\epsilon} = [(c+\Delta l_x) - (c-\Delta x_t)]/c = \Delta\bar{l}_x + \Delta\bar{x}_t \tag{41}$$

From Eqs. (6) and (12), the slackness ratio becomes

$$\bar{\epsilon} = \tfrac{1}{2}\int_0^1\left(\frac{\partial\zeta}{\partial\xi}\right)^2 d\xi \tag{42}$$

The vertical deflection of the trailing edge z_t produces a local aerodynamic twist in the wing α_T. The small angle approximation is

$$\alpha_T = -z_t/c = -\bar{z}_t \tag{43}$$

The camber and twist combine as an effective sail angle of attack;

$$\alpha_s = \alpha_\epsilon + \alpha_T,\ (\alpha_\epsilon = K_\epsilon\bar{\epsilon}^{1/2}) \tag{44}$$

Equations (42) and (43) can be evaluated (see Ref. 2 for details) knowing the deflections of the sail and trailing edge derived in section 2;

$$\alpha_s = \pi z_o[K_\epsilon/2 - 2\bar{\delta}_o/\pi - \pi^2 z_o^2/8]\sin\pi\eta \tag{45}$$

An important feature of Eq. (45) is that it shows sail and trailing-edge deflections produce a sinusoidal spanwise distribution in effective aerodynamic angle of attack. The magnitude is to the first order proportional to the sail deflection z_o. For convenience, the magnitude portion of Eq. (26) is defined by a new variable;

$$\alpha_s = \bar{\alpha}_s \sin\pi\eta \tag{46}$$

The parameter $\bar{\alpha}_s$ will be referred to as the sail angle of attack

and becomes, after substituting Eq. (32) for z_o,

$$\bar{\alpha}_s = G\bar{L}(K_\epsilon/2 - 2\bar{\delta}_o/\pi - \pi^2 z_o^2/8)/4\beta\pi\bar{t}_x(1 + \gamma^2) \quad (47)$$

As this equation indicates, the value of lift $\bar{L}$ remains arbitrary, but we may still proceed to investigate the effect of the sinusoidal angle-of-attack distribution.

Spanwise Aerodynamic Loading

The influence of the spanwise variation of the effective sail angle of attack α_s on the lift coefficient, spanwise loading, and induced drag has been determined using Prandtl lifting-line theory. The ratio $\bar{\alpha}_s/\alpha$ is sufficient to completely specify these properties. For instance, the lift coefficient is

$$C_L = C_{L_\alpha}\bar{\alpha} + C_{L_{\bar{\alpha}_s}}\bar{\alpha}_s \quad (48)$$

The effect of sail cambering is embodied in the term $C_{L_{\bar{\alpha}}}$, and C_{L_α} is the usual rigid wing term. An interesting result of lifting-line theory confirms the experimental evidence presented earlier regarding sailwing aerodynamic efficiency. The induced drag factor δ is presented in Fig. 6. We see that for rectangular planforms, reasonable sail deflections ($0 < \bar{\alpha}_s/\alpha < 1$) actually reduce the induced drag compared to a rigid wing ($\bar{\alpha}_s/\alpha = 0$). However, for excessively large sail deflections, a large drag penalty will be incurred.

4. Combined Structural and Aerodynamic Analysis

Up to this point, we have developed expressions for the deflections and induced tensions of the sailwing for arbitrary values of $\bar{L}$, the nondimensional lift. These results have been incorporated in the aerodynamic analysis to develop the parameter $\bar{\alpha}_s$, which in turn is a function of $\bar{L}$. The following analysis will remove the necessity for arbitrary specification of $\bar{L}$. First, we define the parameter ψ by the equation

$$\bar{\alpha}_s = \bar{L}\psi, \ \bar{L} = L/T_o = C_L/C_{T_o} \quad (49)$$

Equations (47) and (49) yield

$$\psi = G(K_\epsilon/2 - 2\bar{\delta}_o/\pi - \pi^2 z_o^2/8)/4\beta\pi\bar{t}_x(1 + \gamma^2) \quad (50)$$

Noting that for $\bar{L} = 0$, we can define $\psi_o = \psi(L = 0)$ and obtain

$$\psi/\psi_o = (1/\bar{t}_x^2)[(1 + \gamma_o^2)/(1 + \gamma^2)]\{1 - [\pi^3 z_o^2/4(\pi K_\epsilon - 4\bar{\delta}_o)]\} \quad (51)$$

This parameter can be seen to be dependent on $\bar{L}$ only, as the induced tensions are also functions of $\bar{L}$. In fact, a representative example of Eq. (51) is plotted in Fig. 5 with the induced tension results. Continuing, Eq. (48) can be written

$$C_L = C_{L_\alpha}\alpha + C_{L_{\bar{\alpha}_s}}\psi_o(C_L/C_{T_o})(\psi/\psi_o) \quad (52)$$

This result relates the sailwing aerodynamics (represented by C_L) to the structural properties (represented by ψ/ψ_o) as desired. An appreciation of the linear and nonlinear contributors to the C_L vs α curve of the sailwing is also afforded by this equation. For constant $q(C_{T_o}$ constant), the $C_{L_{\bar{\alpha}_s}}\psi_o\ C_L/C_{T_o}$ portion represents the linear contribution of sail deflection, whereas the ψ/ψ_o factor represents the nonlinear contribution. Since ψ/ψ_o is determined by the Stiffness number values, it can be said that the nonlinearity of the sailwing lift curve is due entirely to the elastic properties.

Aeroelastic Divergence

The problem of sail instability mentioned earlier is one of aeroelastic divergence and will be investigated with Eq. (52). This condition exists when the internal membrane tensions resisting sail cambering are overcome by opposing aerodynamic lift associated with this camber. Since the membrane tensions are nonlinear, the mathematical definition of divergence will be restricted to the limiting case of zero lift. Divergence will be defined as the point where the rate of change of lift coefficient with the angle of attack for constant dynamic pressure becomes infinite. Eq. (52) is first differentiated with respect to α (for constant q).

The initial lift curve slope ($C_L = 0$, $\psi/\psi_o = 1$) becomes

$$\left(\frac{\partial C_L}{\partial\alpha}\right)_{q|_o} = \frac{C_{L_\alpha}}{1 - (C_{L_{\bar{\alpha}_s}}/C_{T_o})\psi_o} \quad (53)$$

The divergence tension coefficient ($C_{T_o} = C_{T_{o_d}}$) is obtained from the condition when the initial lift curve slope is infinite;

$$C_{T_{o_d}} = C_{L_{\bar{\alpha}_s}}\psi_o \quad (54)$$

and

$$C_{T_{o_d}} = \frac{C_{L_{\bar{\alpha}_s}}G}{4\beta\pi(1 + \gamma_o^2)}\left[\frac{K_\epsilon}{2} - \frac{2\bar{\delta}_o}{\pi}\right], \ \gamma_o^2 = 4R_o/AR^2 \quad (55)$$

Equation (55) shows that the divergence tension coefficient depends primarily on aspect ratio (via $C_{L_{\bar{\alpha}_s}}$) and the trailing-edge shape parameter β. High aspect ratios and trailing-edge shapes of small curvature are most prone to divergence. Only one Stiffness number R_o is contained in Eq. (55), and it is independent of the elastic parameters K_s and K_w. Therefore, the divergence properties of the sailwing are not influenced by the sail and trailing-edge elastic properties. Finally, since neither T_o or q can independently specify $C_{T_{o_d}}$, a "divergence speed" is only uniquely determined by a particular pre-tension T_o.

It should be stressed that the previously mentioned results were obtained by holding dynamic pressure constant during differentiation. If this condition is relaxed, and a constant lift $\bar{L}$ constraint substituted in its place, the nature of the lift curve slope equation is significantly altered. For a flight vehicle, the constant lift condition corresponds to steady level flight and is therefore of primary interest. We immediately obtain a new result by differentiating Eq. (52) again:

$$(\partial C_L/\partial\alpha)_{\bar{L}} = C_{L_\alpha} \quad (56)$$

Now the lift curve slope for constant lift conditions becomes identical to that of the corresponding rigid wing, and it can be concluded that the static stability and control of sailwing equipped aircraft will differ little from conventional types.

Nonlinear Lift Curve

The final goal of this analysis is an equation for the nonlinear C_L vs α lift curve of the sailwing. This can be accomplished by substituting Eq. (54) in Eq. (52) and solving

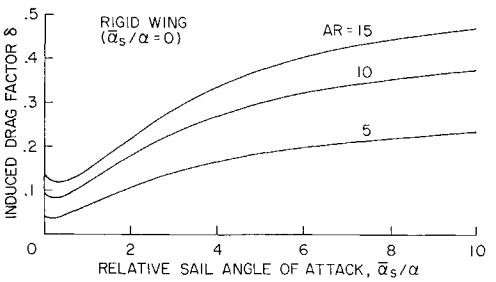

Fig. 6 Sailwing drag fraction in excess of the minimum induced drag for an elliptical lift distribution.

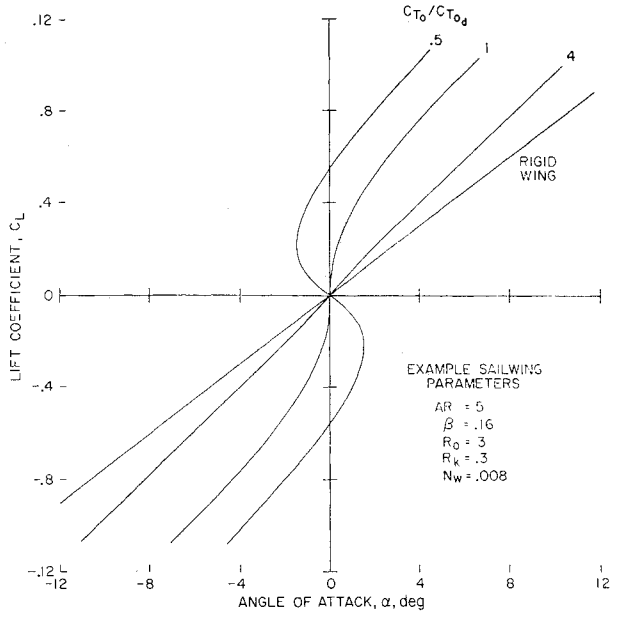

Fig. 7 Effect of dynamic pressure on the theoretical sailwing lift curves.

for α:

$$\alpha = (C_L/C_{L_\alpha})[1 - (\psi/\psi_o/C_{T_o}/C_{T_{o_d}})] \qquad (57)$$

Figure 7 illustrates this equation for several dynamic pressures. For low speeds (or high pre-tension) $C_{T_o} \gg C_{T_{o_d}}$ the lift curve is similar to the rigid wing case, and the nonlinearity is small. For $C_{T_o} = C_{T_{o_d}}$, the initial slope is infinite, but the nonlinear effect (ψ/ψ_o), caused by the growing induced tensions stiffening the sail, tends to stabilize the lift curve. At even higher dynamic pressures, the nonlinear effects are predominant. At high angles of attack, the lift curve is stable, but near zero lift the multiple valued lift curves would produce hysteresis loops.

5. Experimental Results

To provide a basis for judging the validity of the aforementioned analysis, a few experimental results will now be discussed. A small (3.33 ft) wind-tunnel model was specially designed and tested for this purpose. A symmetrical airfoil section was formed by a cylindrical leading-edge spar and a doubly wrapped sail surface. Internal tensions were measured by strain gage instrumentation, and external static pressure surveys were used to determine the span lift distribution. A photograph of the model being tested in the wind tunnel is given in Fig. 8. The deformation of the upper-wing surface is apparent and indicates the typical sailwing results obtained with this model. Complete results are reported in Ref. 2.

The first example in Fig. 9 presents measured induced tensions in the sail and the trailing edge for several dynamic pressures. At each q, the angle of attack was used to vary the model lift. Note that the experimental results are substantially independent of q as predicted by the theory. It should be pointed out that a modified form of Eq. (36) for $\Delta\bar{T}$ has been used, which gives better correlation with experimental results. The modification involves eliminating the smaller contributor to the trailing-edge tension $[(1/4)\pi^2\bar{\delta}_o]$ due to the vertical deflection z_t. The nonlinear variation of the induced tensions is well evidenced by the experimental results, which is in agreement with the theory. For low values of q which correspond to small lift values, the induced tensions are nearly linear with $\bar{L}^2$. As lift increases, the nonlinearity becomes increasingly apparent.

Figure 10a illustrates the correlation of aeroelastic divergence calculations. The theoretical variation with Stiffness number R_o (ratio of spanwise to chordwise pre-tension, t_{y_o}/t_{x_o}) results from the fact that for a given chordwise pre-tension t_{x_o}, increasing spanwise pre-tension further stiffens the sail and reduces $C_{T_{o_d}}$ by making it more resistant to aerodynamic forces. The experimental values were obtained by extrapolating the measured data and generally confirm the theoretical results. Their somewhat lower values are probably caused by the low Reynolds numbers degrading the ideal potential theory aerodynamic effectiveness of camber and angle of attack. The effects of boundary-layer separation would tend to reduce the values of $C_{L_{\bar{\alpha}_s}}$ and K_ϵ used in Eq. (55) for $C_{T_{o_d}}$.

Figure 10b illustrates a typical sailwing characteristic, the high lift curve slope under constant q conditions. The experimental values were determined directly from the slope at the origin of C_L vs α plots. The dynamic pressure variation for a given pre-tension yielded the C_{T_o} variation, and the divergence values were the experimentally determined ones shown in Fig. 10a. The rapid approach to divergence is illustrated graphically by this figure as $C_{T_o}/C_{T_{o_d}}$ nears a value of 1.0. The correlation of results with theory is generally satisfactory except in the region $C_{T_o}/C_{T_{o_d}} = 2$. It is suspected that the single harmonic loading assumption on which the membrane deflection theory is based, is the primary reason for this discrepancy.

A brief examination of the spanwise lift distribution is afforded by Fig. 11. The results of lifting line theory clearly show the increase in lift near the midsemispan resulting from the deformation of the sail surface. The experimental values were obtained by integrating chordwise pressure distributions, and also confirm the effects of the sail deformation.

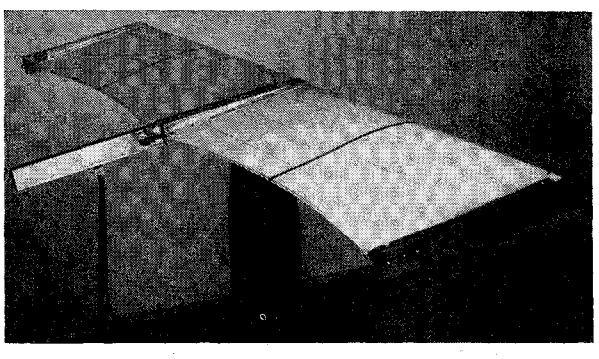

Fig. 8 Experimental wind-tunnel model, q = 10.4 PSF, C_L = 0.888.

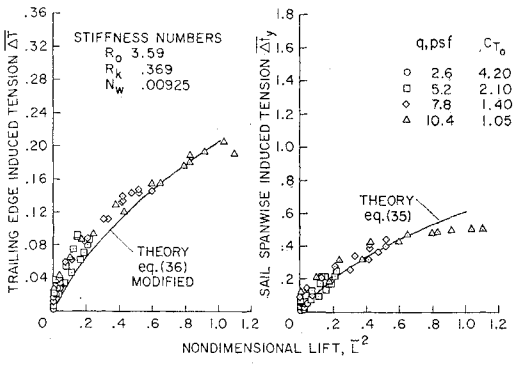

Fig. 9 Comparison of experimentally measured sail spanwise and trailing-edge induced tensions with theory.

6. Some Design Considerations for Sailwing Applications

The foregoing analysis and experimental results were intended to provide insight into some important characteristics of the sailwing. The purpose of the following discussion is to examine one consequence of this analysis having significant ramifications regarding the structural design of practical sailwings. The importance of the trailing-edge pre-tension and induced tensions for structural design of the sailwing will be demonstrated with a simple equation. Assuming the desirability of operating at all times above the divergence tension coefficient, the trailing-edge pre-tension must be equal or greater than

$$T_o = C_{T_{o_d}} q_{\max} S_w \tag{58}$$

For steady level flight at minimum speed

$$W = C_{L_{\max}} q_{\min} S_w \tag{59}$$

Combining these equations yields

$$T_o/W = (q_{\max}/q_{\min}) C_{T_{o_d}}/C_{L_{\max}} \tag{60}$$

Therefore, at the stall speed, for a typical value of the ratio $C_{T_{o_d}}/C_{L_{\max}} = 0.5$, the trailing-edge pre-tension will be equal to one-half the weight of the aircraft. Its magnitude can be seen to increase with the square of the maximum velocity. Therefore, the structural design problems of the sailwing for moderate speed applications may be difficult. However, two factors are present which have a large effect on this conclusion. Unlike conventional rigid wings, it may be feasible to operate the nonlinear sailwing within the divergence condition. As depicted in Fig. 8, low angles of attack would have to be avoided. Under these conditions, the sailwing would rely on lift to provide sail stability, much the same as non-pre-tensioned semirigid flexible wings (i.e., the parawing), and still retain its excellent lift-drag ratio.

Another possibility for reducing the pre-tension requirement is to modify the structure. A trailing-edge bridle system, or a midsemispan rib are two approaches. Another would be to increase the spar chordwise depth, reducing the percentage chord comprising the sail and thus, reducing $C_{T_{o_d}}$ by virtue of decreased aerodynamic effectiveness.

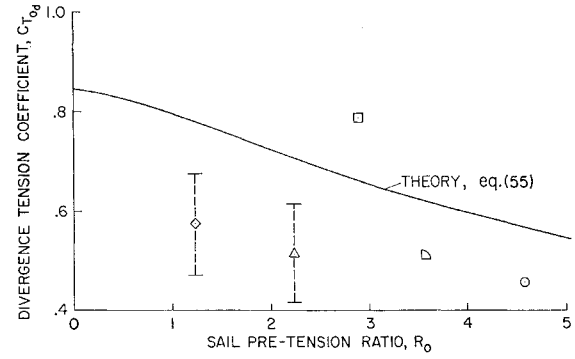

a) Divergence tension coefficient

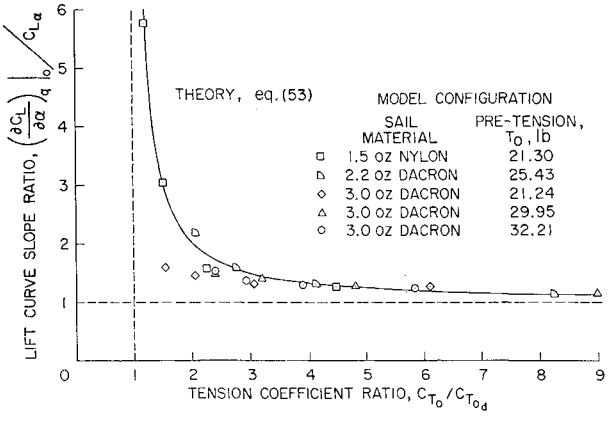

b) Initial lift curve slope

Fig. 10 Experimental comparisons for several combinations of sail material and trailing-edge pre-tension.

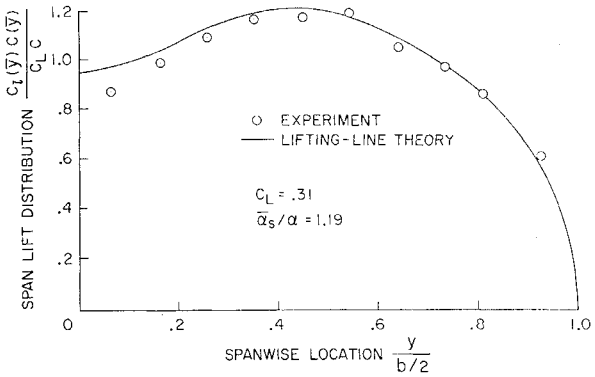

Fig. 11 Comparison of experimental span lift distribution with theory.

7. Conclusions

The principal results of this analysis will be summarized at this point:

1) Lifting-line theory substantiates the high sailwing maximum lift-drag ratios which have been observed experimentally.

2) The nonlinear behavior of the sailwing is due to the elastic properties of the sail- and trailing-edge member.

3) The aeroelastic divergence coefficient is independent of elastic properties, and is only related to geometric factors and the sail pre-tension ratio.

4) Two conditions are identified which yield widely differing values for lift curve slope, the constant lift and constant q cases.

5) The nonlinear lift curves show that operation beyond divergence is possible, but also that hysteresis loops in the lift curve may exist.

References

[1] Sweeney, T. E., "Exploratory Sailwing Research at Princeton," Rept. No. 578, Dec. 1961, Princeton University, Department of Aerospace and Mechanical Sciences, Princeton, N. J.

[2] Ormiston, R. A., "Theoretical and Experimental Aerodynamics of an Elastic Sailwing," Ph.D. thesis, Oct. 1969, Department of Aerospace and Mechanical Sciences, Princeton University, Princeton, N. J.

[3] Fink, M. P., "Full-Scale Investigation of the Aerodynamic Characteristics of a Model Employing a Sailwing Concept," TN D-4062, July 1967, NASA.

[4] Fink, M. P., "Full-Scale Investigation of the Aerodynamic Characteristics of a Sailwing of Aspect Ratio 5.9," TN D-5047, Feb. 1969, NASA.

[5] Sibert, G. W., "A Flight Test Study of the Lift and Drag Characteristics of Sailwing IV," Rept. 780, May 1966, Princeton University, Department of Aerospace and Mechanical Sciences, Princeton, N. J.

[6] Condit, P. M., "Lateral Control of the Sailwing," Rept. 734, May 1965, Princeton University, Department of Aerospace and Mechanical Sciences, Princeton, N. J.

[7] Herrick, G. E., "Lateral Control of a Rectangular Sailwing," MS thesis, May 1964, Department of Aeronautics and

Astronautics, Massachusetts Institute of Technology, Cambridge, Mass.

[8] Ormiston, R. A. and Fox, R. D., "The Sailwing Lifting Body Concept," Rept. 828, Feb. 1968, Princeton University, Department of Aerospace and Mechanical Sciences, Princeton, N. J.

[9] Polhamus, E. C. and Naeseth, R. L., "Experimental and Theoretical Studies of the Effects of Camber and Twist on the Aerodynamic Characteristics of Parawings Having Nominal Aspect Ratios of 3 and 6," TN D-972, 1963, NASA.

[10] Bugg, F. M., "Effects of Aspect Ratio and Canopy Shape on Low-Speed Aerodynamic Characteristics of 50.0° Swept Parawings," TN D-2992, July 1965, NASA.

[11] Burnell, J. A. and Nielsen, J. N., "Theoretical Aerodynamics of Flexible Wings at Low Speeds, IV-Experimental Program and Comparison with Theory," Vidya Rept. 172, Feb. 1965, Vidya Division, Itek Corporation, Palo Alto, Calif.

[12] Croom, D. R., Naeseth, R. L., and Sleeman, N. C., Jr., "Effects of Canopy Shape on Low Speed Aerodynamic Characteristics of a 55° Swept Parawing with Large-Diameter Leading Edges," TN D-2551, 1964, NASA.

[13] Naeseth, R. L. and Fournier, P. G., "Low Speed Wind Tunnel Investigation of Tension Structure Parawings," TN D-3940, June 1967, NASA.

[14] Barte, G. R., Jr., "Flexible Wings for Maneuvering and Landing Application in the De-Coupled Concept," AIAA Paper No. 67-200, New York, 1967.

[15] Burk, S. M., Jr. and Ware, G. M., "Static Aerodynamic Characteristics of Three Ram-Air-Inflated Low-Aspect Ratio Fabric Wings," TN D-4182, Sept. 1967, NASA.

[16] Thwaites, B., "The Aerodynamic Theory of Sails I. Two-Dimensional Sails," *Proceedings of the Royal Society*, Ser. A, Vol. 261, 1961, pp. 402–442.

[17] Nielsen, J. N., "Theory of Flexible Aerodynamic Surfaces," *Journal of Applied Mechanics*, Ser. E., Vol. 30, No. 3, Sept. 1963, pp. 435–442.

FEBRUARY 1971 J. AIRCRAFT VOL. 8, NO. 2

Transonic Airfoil Design

M. S. Cahn* and J. R. Garcia†
Northrop Corporation, Hawthorne, Calif.

A method recently developed by Northrop consists of a computer program which will determine an airfoil shape from predetermined supercritical velocity distributions having extensive regions of supersonic flow. The velocity is given vs the distance around the airfoil. This allows a designer to design to a given lift by specifying the required circulation. Also, boundary-layer problems can be avoided by restricting adverse velocity gradients. Starting with a given compressible pressure or velocity distribution with mixed subsonic and supersonic regions, an airfoil shape can be determined. This is done by making a transformation that causes the streamline and potential line network to give an equivalent incompressible flow. This incompressible problem is then solved by complex function theory, and the solution is transformed back to the compressible plane. A computer program using this method has been applied to several shapes with known solutions. Agreement between calculated shapes and actual shapes was excellent. A 4.6% airfoil was designed from a prescribed velocity distribution and tested in the wind tunnel at transonic speeds. Good agreement was obtained between theoretical and experimental results. Transonic airfoils can be designed by this method.

Nomenclature

a^* = speed of sound at Mach one
C_L = lift coefficient
C_M = pitching moment coefficient
C_P = pressure coefficient
Im = imaginary part
M = Mach number
n = distance normal to streamline
Re = real part
s = distance along streamline
V = local velocity
V_∞ = freestream velocity
Z_c = complex coordinate in compressible plane
Z_i = complex coordinate in incompressible plane
α = local flow angle in airfoil plane
ϵ_T = trailing-edge angle
ζ = complex coordinate in circle plane
θ = angle in circle plane
ρ = density
ρ_0 = stagnation density
ϕ = velocity potential
ψ = stream function

Subscripts

c = compressible
i = incompressible

Received February 11, 1970; revision received June 15, 1970.

* Manager, Applied Aerodynamics and Performance, Aircraft Division. Member AIAA.

† Research Aerodynamicist, Aircraft Division.

Introduction

If aircraft flight speed approaches the speed of sound, the air flowing around the aircraft will be mixed supersonic and subsonic flow. The equations for calculating the flow and its resultant effects on the forces on a body are radically different for supersonic and subsonic speeds. When a flow problem consists of a mixture of both types of flow, the resulting problem becomes very difficult. As a result, scientists and engineers concerned with the development of modern aircraft rely heavily on empirical techniques and wind-tunnel test results.

The state-of-the-art today is rapidly progressing. Several years ago Pearcey[1] at the National Physics Laboratory in England noticed that some wings being tested in the wind tunnel exhibited at certain conditions the property of induc-